

# Particle Characteristics and Metal Release from Natural Rutile (TiO<sub>2</sub>) and Zircon Particles in Synthetic Body Fluids

Yolanda Hedberg\*, Jonas Hedberg, Inger Odnevall Wallinder

Division of Surface and Corrosion Science, Department of Chemistry, Royal Institute of Technology (KTH), Stockholm, Sweden.  
Email: \*yolanda@kth.se

Received October 17<sup>th</sup>, 2011; revised November 18<sup>th</sup>, 2011; accepted December 8<sup>th</sup>, 2011

## ABSTRACT

Titanium oxide (rutile, TiO<sub>2</sub>) and zircon (ZrSiO<sub>4</sub>), known insoluble ceramic materials, are commonly used for coatings of implant materials. We investigate the release of zirconium, titanium, aluminum, iron, and silicon from different micron-sized powders of 6 powders of natural rutile (TiO<sub>2</sub>) and zircon (ZrSiO<sub>4</sub>) from a surface perspective. The investigation includes five different synthetic body fluids and two time periods of exposure, 2 and 24 hours. The solution chemicals rather than pH are important for the release of zirconium. When exceeding a critical amount of aluminum and silicon in the surface oxide, the particles seem to be protected from selective pH-specific release at neutral or weakly alkaline pH. The importance of bulk and surface composition and individual changes between different kinds of the same material is elucidated. Changes in material properties and metal release characteristics with particle size are presented for zircon.

**Keywords:** Rutile; Zircon; Metal Ion Release; Particles; Surface Analysis

## 1. Introduction

Titanium oxide (rutile, TiO<sub>2</sub>) and zircon (ZrSiO<sub>4</sub>), known insoluble ceramic materials [1-5], play a large role for implant materials and corrosion protection (coating) of implant materials [2,5,6]. For example, the spontaneous growth of rutile on titanium-based implant surfaces is favorable from a biocompatibility perspective and reduces furthermore the extent of metal release. Even though stated insoluble, very low amounts of metals, depending on the surrounding solution (e.g. the solution pH), have been reported to be released in human body fluids [3-5]. Potential adverse effects induced by particles (e.g. released from implant materials) of rutile and zirconia (ZrO<sub>2</sub>) have been studied in the literature and mostly ascribed to their particle characteristics (size and shape), rather than to their solubility [1,7,8]. Adverse effects have also been reported for nanometer-sized [8-12] and micron-sized particles [1,8,12] of anatase (TiO<sub>2</sub>) of slightly lower solubility compared with rutile [3]. When the particles are small enough to be phagocytized (<5 μm), they show a significant increase in toxic response [1,8]. Below this size limit, cytotoxicity for anatase and rutile TiO<sub>2</sub> and for ZrO<sub>2</sub> particles (pigments) has been reported to be size-independent when normalized to volume, but to increase with increasing particle size when normalized to surface area or

particle number [8]. However, no surface area or size dependence of pulmonary toxicity in rats have been observed for TiO<sub>2</sub> pigments of different structure and size (10 to 300 nm) [13]. The lack of surface area dependence on toxicity for nanometer sized particles has also been observed for TiO<sub>2</sub> nanoparticles [14] showing a higher (100 times) cytotoxicity for anatase compared to rutile TiO<sub>2</sub> pigments. The structure of TiO<sub>2</sub> was reported important for the induced toxicity with slightly higher levels of oxidative DNA damage induced by a mixture of rutile and anatase ultrafine particles compared with anatase or rutile alone [15]. Examples of reported adverse effects caused by nano- and micron-sized particles of TiO<sub>2</sub> and ZrO<sub>2</sub> observed in vitro and in vivo are cytotoxicity [1,7-8,14], DNA damage [12,15], release of inflammatory cytokines from macrophages [6], liver function damage in mice [9], oxidative stress in the brain of mice [11], decreased recognition memory in mice [10], and toxicological effects on major organs and knee joints of rats [16]. However, compared with other nano- or micron-sized particles, observed acute toxicity is generally low [12,17].

Literature on release mechanisms of rutile, zirconia, or zircon particles in human or artificial body fluids is however scarce, mainly due to their very low solubility. It is evident that the growth of titanium dioxide (rutile structure in comparison to anatase structure) on titanium implant materials reduces the release of soluble titanium species [2,5] and improves its biocompatibility properties [6].

\*Corresponding author.

Rutile and anatase particles (TiO<sub>2</sub>) have been shown soluble up to 0.2% - 1.2% in very acidic aqueous solutions when boiled for 30 minutes [3]. After 30 days in serum, implant materials have shown titanium to be released to an extent of 3.5% of the material (titanium) and 4.6% (TiAl6V4) [18]. Other investigations have focused on the dissolution kinetics of micron-sized zircon particles [4], for example at 25°C in distilled water at pH 5.0 up to 714 hours. Non-measurable levels of dissolved zirconium (while silicon could be measured) were explained by the precipitation of ZrO<sub>2</sub> and later ZrSiO<sub>4</sub>.

Toxicity studies alone can however neither explain observed differences in the induced toxic response of “insoluble” particles of different structure nor their induced toxicity when taken up by the cell or when remaining in the tissue over a long time period. Such investigations require additional studies on material properties in vivo, studies of the change of surface properties such as structure, composition and charge, and studies on the mechanisms of metal release.

Several factors may be important for the metal release mechanism of rutile and zircon particles in the human body: 1) surface structure and composition; 2) solution pH; 3) solution composition, including organic species, proteins, oxidants and reductants. Ligand-induced metal release mechanisms, expected to play an important role in vivo and in complexing artificial solutions [19], have been shown to be dependent on protein adsorption and zeta potential of the particles, parameters both influenced by pH and surrounding chemical species (e.g. Ca ions) [20] and by the surface structure [21].

In this study, we investigate the release of zirconium, titanium, aluminum, iron, and silicon from different natural micron-sized (median diameter 104 µm - 130 µm) rutile (TiO<sub>2</sub>, 2 types) and zircon (ZrSiO<sub>4</sub>, 4 types, of which one was micronized to less than 6 µm) powders. Main focus of the investigation is placed on the importance of bulk and surface composition for the release mechanisms into five different artificial body fluids covering a pH range from 1.5 to 7.4 (different possible endpoints), and with different solution complexities (artificial gastric fluid, artificial lysosomal fluid, artificial sweat, phosphate buffered saline, and Gamble’s solution). Generated metal release data were performed within the Registration, Evaluation and Authorisation of Chemicals (REACH) regulation even if rutile and zircon were exempt from REACH as they are naturally occurring substances. They were therefore mainly investigated to reach a deeper understanding of chemical-physical properties of these materials.

## 2. Materials and Methods

### 2.1. Materials and Particle Characterization

Six different materials, 2 natural rutile (TiO<sub>2</sub>) and 4 zircon powders were investigated, denoted “a”, “b”, “c”, “d”,

“e”, and “f” (micronized zircon < 6 µm).

The specific surface area (m<sup>2</sup>/g) per mass unit was determined by means of BET-analysis (adsorption of nitrogen at cryogenic condition) using a Micromeritics Gemini V instrument. Nitrogen adsorption measurements were performed at five different partial pressures (p/p<sub>0</sub> 0.10 - 0.25) with a standard deviation between replicas of less than 1%. The specific surface area of all particles is given in **Table 1**.

Triplicate measurements of particle size distribution in solution (PBS, see next section for composition) were conducted by means of laser diffraction using a Malvern Mastersizer 2000 equipment with a Hydro SM dispersion unit. Refractive indices of zirconium dioxide or titanium dioxide, and water (since it was the solvent of the test medium), were used as input parameters applying standard operational conditions. In **Table 2**, the measured median particle diameter, and the 10% and 90% size distribution cut off points (by volume%) are presented for the different particles.

Surface compositional analyses were performed by means of X-ray Photoelectron Spectroscopy, XPS. Spectra were recorded using a Kratos AXIS UltraDLD x-ray photoelectron spectrometer (Kratos Analytical, Manchester, UK) using a monochromatic Al x-ray source (150 W) on areas approximately sized 700 × 300 µm. Wide spectra were run to detect elements present in the outermost surface of the test items. Wide and detailed high resolution spectra (20 eV pass energy) were acquired for carbon (C 1s), oxygen (O 1s), zirconium (Zr 3d), silicon (Si 2p), titanium (Ti 2p), iron (Fe 2p) and aluminium (Al 2p).

**Table 1.** Specific surface area [m<sup>2</sup>/g], measured by means of BET.

Material	a	b	c	d	e	f
BET area	3.16*	1.19	1.03	0.84	0.65	5.97

\*This value is higher as expected from SEM and laser diffraction results.

**Table 2.** Measured median particle diameter (d<sub>0,5</sub>) and the 10% (d<sub>0,1</sub>) and 90% (d<sub>0,9</sub>) size distribution percentiles, presented as a percentage of volume (mass) of the different particles in PBS using LD.

Material name	d <sub>0,1</sub> [µm]	d <sub>0,5</sub> [µm]	d <sub>0,9</sub> [µm]
a	74	104	147
b	73	105	158
c	80	125	199
d	91	130	188
e	85	129	194
f	0.6	1.7	5.7

The test items were fixed on copper tape to avoid any dispersion of the powder particles in the vacuum inside the instrument chamber. All binding energies were calibrated by assigning the carbon C1s contamination peak to 285 eV. All peak areas were determined by assigning a linear baseline. Average results were calculated from several local areas, for each powder, respectively.

Differences in surface morphology of the investigated particles were studied using a tabletop scanning electron microscope (SEM) with backscattered electrons (Hitachi TM-1000). The powder samples were fixed on carbon tape to avoid any dispersion of particles inside the instrument chamber and to assure appropriate conduction. The morphology is shown in **Figure 1** for all materials.

The chemical composition and structure (bulk information) of the materials were investigated by means of Raman spectroscopy in reflection mode. This configuration is in essence similar to the Total Internal Reflection Raman spectrometer described elsewhere [22]. Briefly, a highly stable 532 nm laser (Quantum lasers) is delivered to the sample in an external reflection configuration at an angle of incidence of 78 degrees. The polarization of the beam was S (perpendicular to the plane of incidence). The Raman scattered light is collected using an ultra-long high numerical aperture objective with 50×

magnification attached to a modified upright Axio microscope from Zeiss. The scattered light is then passed through a sharp long pass filter that blocks the 532 nm light and finally focused to a spectrograph (ShamrockAndor) and detected with a CCD camera (Newton 940Andor).

## 2.2. Test Fluids

The powders were exposed to five different test fluids at a pH range from 1.6 to 7.4. The composition of the fluids and the pH prior to and after exposure is given in **Table 3**. The solutions were selected to cover a wide and relevant

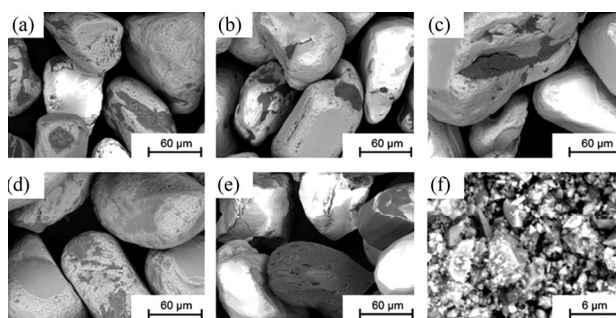


**Figure 1.** SEM images (backscattered electrons) at a magnification of 1000× (powders (a) to (e)) and 10,000× (powder (f)).

**Table 3.** Composition of the different synthetic body fluids (in g/L), pH adjustment, and pH prior and after exposure.

Chemical	PBS	GMB	ALF	ASW	GST
MgCl <sub>2</sub>	-	0.0953	0.0497	-	-
NaCl	8.77	6.0193	3.210	5.0	-
KCl	-	0.2982	-	-	-
Na <sub>2</sub> HPO <sub>4</sub>	1.28	0.126	0.071	-	-
Na <sub>2</sub> SO <sub>4</sub>	-	0.063	0.039	-	-
CaCl·2H <sub>2</sub> O	-	0.3676	0.128	-	-
C <sub>2</sub> H <sub>3</sub> O <sub>2</sub> Na·H <sub>2</sub> O (sodium acetate)	-	0.7005	-	-	-
NaHCO <sub>3</sub>	-	2.6043	-	-	-
C <sub>6</sub> H <sub>5</sub> Na <sub>3</sub> O <sub>7</sub> ·2H <sub>2</sub> O (sodium citrate)	-	0.097	0.077	-	-
NaOH	-	-	6.000	-	-
Citric acid	-	-	20.80	-	-
Glycine	-	-	0.059	-	-
C <sub>4</sub> H <sub>4</sub> O <sub>6</sub> Na <sub>2</sub> ·2H <sub>2</sub> O (Na <sub>2</sub> Tartrate·2H <sub>2</sub> O)	-	-	0.090	-	-
C <sub>3</sub> H <sub>5</sub> NaO <sub>3</sub> (NaLactate)	-	-	0.085	-	-
C <sub>3</sub> H <sub>5</sub> O <sub>3</sub> Na (NaPyruvate)	-	-	0.086	-	-
(NH <sub>2</sub> ) <sub>2</sub> CO (urea)	-	-	-	1.0	-
CH <sub>3</sub> CHOHCO <sub>2</sub> H (lactic acid)	-	-	-	1.0	-
KH <sub>2</sub> PO <sub>4</sub>	1.36	-	-	-	-
25% HCl	-	-	-	-	4.0
pH adjusted with	370 μL/L 50% NaOH	260 μL/L 25% HCl	1.7 mL/L 50% NaOH	1% ammonia	-
Initial pH	7.38	7.40 - 7.43	4.47 - 4.48	6.47 - 6.62	1.67
Final pH (2h)	7.39 - 7.42	7.66 - 7.91	4.45 - 4.47	6.15 - 6.32	1.44 - 1.50
Final pH (24h)	7.36 - 7.43	7.88 - 8.66	4.43-4.46	5.59 - 5.72	1.44 - 1.53

PBS—Phosphate buffered saline; GMB—Gamble's solution; ALF—artificial lysosomal fluid; ASW—artificial sweat; GST—artificial gastric fluid.

range of pH and relevant artificial body fluids for human exposure via inhalation, ingestion, and skin contact. Phosphate-buffered saline (PBS, pH 7.4) is a standard physiological solution that mimics the ionic strength of human blood serum. Gamble's solution (GMB, pH 7.4) mimics the interstitial fluid within the deep lung under normal health conditions [23]. Artificial sweat (ASW, pH 6.5) simulates the hypoosmolar fluid, linked to hyponatraemia (loss of Na<sup>+</sup> from blood), which is excreted from the body upon sweating [24]. Artificial lysosomal fluid (ALF, pH 4.5) mimics intracellular conditions in lung cells occurring in conjunction with phagocytosis and represents relatively harsh conditions [25]. Artificial gastric fluid (GST, pH 1.6) simulates the very harsh digestion environment of high acidity in the stomach [26].

### 2.3. Experimental Procedure and Metal Analysis

Triplicate samples were prepared for exposure in different test fluids, each for two different time periods. In addition, one blank sample (without addition of any particles) containing only the test solution was incubated together with the triplicate samples for each time period.  $5 \pm 0.5$  mg of each material was weighed using a Mettler AT20 balance with readability of 2 µg, and placed in a PMP Nalge® jar. 50 mL of the test solution was then added to the Nalge® jar containing the material of interest, before incubated in a Platform-Rocker incubator SI 80 regulated at  $37^\circ\text{C} \pm 0.5^\circ\text{C}$ . The solution was gently shaken (bi-linearly) with an intensity of 25 cycles per minute for 2 and 24 hours, respectively. After exposure, the samples were allowed to cool to ambient room temperature before the final pH of the test solution was measured. The test fluid was then separated from the powder particles by centrifugation at 3000 rpm for 10 minutes (704 relative centrifugal force, r.c.f.), resulting in a visually clear supernatant with remaining particles in the bottom of the centrifuging tube. The supernatant solution was decanted into a polypropylene storage flask and acidified to a pH less than 2 (not required in the case of artificial gastric fluid) with 65% pure HNO<sub>3</sub> prior to solution analysis. All vessels for exposure, centrifugation and storage of samples were acid-cleaned in 10% HNO<sub>3</sub> for at least 24 hours, then rinsed four times with ultra-pure water and dried in ambient air in the fume hood within a few hours to avoid any risk of contamination.

Dissolved/released concentrations of metals were analysed by means of inductively Coupled Plasma Optical Emission Spectrometry (ICP-OES), using a Varian Vista Ax with an axial plasma with CCD detector using standard operational procedures with multiple standards for calibration and triplicate measurements of each sample (relative standard deviation 1% – 8%). The sample matrixes and standard matrixes were adjusted to the same sodium chlo-

ride content by eventually adding sodium chloride on-line. The released elements considered in this paper are zirconium, titanium, aluminium, iron, and silicon. Calcium, magnesium, and phosphorus, measured to significant extent, were not considered, since these elements are present in the test fluid, are non-toxic, and easily dissolved. Limits of detection (calculated from the three-fold background concentration) for the metal elements taken into account were: Al-0.68 µg/L, Fe-0.80 µg/L, Si-5.1 µg/L, Ti-0.12 µg/L, Zr-0.34 µg/L.

## 3. Results and Discussion

### 3.1. Particle Characterization

The chemical composition and structure of the natural rutile TiO<sub>2</sub> and zircon (ZrSiO<sub>4</sub>) powders were investigated using Raman spectroscopy. Peak positions and relative intensities are given in **Table 4** and Raman spectra shown in **Figure 2**. For the rutile powders (“a” and “d”), main peaks were as expected assigned to rutile TiO<sub>2</sub> (145, 246, 440, 607 cm<sup>-1</sup>) [21,27,28]. Differences in relative peak intensities, and also the occurrence of peaks in the 700 cm<sup>-1</sup> - 800 cm<sup>-1</sup> region for the rutile powder “a” could be due to differences in grain size implying bulk TiO<sub>2</sub> for the rutile particle “d”, and smaller grains (possibly nano-sized) for the rutile powder “a” [29].

The spectra of the zircon powders “b”, “c”, and “e” were similar (**Figure 2**), with main peak positions at approximately 215, 355, 439, 822, 995, 2250, and 2540 cm<sup>-1</sup>, all except the band at 822 cm<sup>-1</sup> assigned to zircon [30]. A significantly different Raman spectrum was generated for the zircon powder “f” with broader and shifted peaks, but also with differences in relative peak intensities when compared with the other three zircon powders “b”, “c”, and “e” (**Figure 2**). The latter three powders revealed few weak bands at 461 cm<sup>-1</sup> (only “b”), at 503 cm<sup>-1</sup> - 510 cm<sup>-1</sup>, and at 572 cm<sup>-1</sup> - 577 cm<sup>-1</sup> (only “c” and “e”), possibly assigned to monoclinic ZrO<sub>2</sub> [31]. The same bands, of significantly stronger relative intensity (462, 510, and 575 cm<sup>-1</sup>), were observed for the micronized zircon powder “f”. The strong peaks observed for the zircon powders “b”, “c”, and “e” were in contrast very weak or not present for the zircon powder “f”. The only exception was that the band at approximately 995 cm<sup>-1</sup> (“b”, “c”, “e”) was slightly shifted to 978 cm<sup>-1</sup> in a broader peak. It is unclear why the zircon powder “f” disclosed a different spectrum. However, similar to the other zircon powders, most peaks were assigned to zircon and monoclinic ZrO<sub>2</sub>. A plausible explanation could be a larger fraction of monoclinic ZrO<sub>2</sub> and smaller grain size (broader peaks), compared with the zircon powders “b”, “c”, and “e” [31].

Differences in bulk (**Table 5**) and surface composition (determined by means of X-ray Photoelectron spectroscopy, XPS), are shown for the investigated powders in

**Table 4. Raman peak positions and relative intensities (strong, medium, weak) of the two rutile powders (“a” and “d”) and the four zircon powders (“b”, “c”, “e”, and “f”). Reference peak positions are included for comparison.**

Material	Peak positions	References
a (rutile)	150 w, 245 s, 440 s, 603 s, 705 m, 800 m, 1632 m	
b (zircon)	154 w, 215 s, 272 w, 351 s, 439 s, 461 w, 503 w, 577 m, 627 m, 711 m, 822 s, 864 w, 965 w, 992 s, 1180 w, 1457 w, 2250 s, 2315 w, 2450 w, 2536 s, 3221 w, 3297 w, 3430 m, 3480 w, 3545 w, 3636 m, 3752 w	
c (zircon)	215 s, 355 s, 438 s, 510 w, 630 w, 712 w, 823 m, 866 w, 970 w, 998 s, 1181 m, 1315 w, 1460 w, 2250 s, 2541 s, 3310 w, 3420 m, 3640 m, 3752 w	
d (rutile)	145 w, 246 s, 440 s, 607 s, 832 w, 1602 w	
e (zircon)	154 w, 218 s, 356 s, 439 s, 474 w, 510 w, 572 w, 592 w, 709 w, 820 m, 868 m, 969 w, 996 s, 1180 m, 1310 w, 1458 w, 2007 w, 2246 s, 2544 s, 3220 w, 3303 w, 3420 m, 3633 m, 3752 m	
f (zircon)	183 w, 267 s, 342 w, 382 w, 462 m, 510 s, 575 s, 620 w, 750 w, 978 s, 1015 w, 3410 w, 3650 w	
	145 s, 243 s, 449 s, 610 s	[21]
	147 s, 236 m, 447 s, 611 s	[28]
rutile TiO <sub>2</sub> (references)	147 w, 235 m, 446 s, 610 s	[27]
	105 s, 237 m, 447 s, 612 m, 700 w (fine crystallites)	[29]
zircon (reference)	202.5, 215.5, 225.5, 265.5, 357.5, 393.5, 439.5, 547, 641.5, 925.5, 975.5, 1009 s	[30]
	145, 268, 314, 463, 604w, 639 (tetragonal)	[40]
ZrO <sub>2</sub> (references)	192, 335, 347, 382, 476s, 617, 638 (monoclinic)	[41]
	101 m, 178 s, 191 s, 224 m, 306 m, 334 s, 350 s, 382 s, 475 s, 504 m, 539 m, 560 m, 618 s, 638 s, 758 w (monoclinic)	[31]
ZrO <sub>2</sub> small grains (5 nm) (reference)	114 m, 178 s, 220 w, 328 m, 338 w, 380 m, 479 m, 534 w, 554 w, 612 m, 704 w, 714 w, 725 w, 760 w, 1038 s	[31]

s—strong, m—medium, w—weak.

**Table 5. Nominal bulk composition [wt%] of natural rutile and zircon powders investigated based on supplier information.**

Material name	TiO <sub>2</sub>	ZrO <sub>2</sub>	SiO <sub>2</sub>	Al <sub>2</sub> O <sub>3</sub>	Fe <sub>2</sub> O <sub>3</sub>	others (>1 wt%)
a	92.8	1.31	2.45	0.51	0.95	-
b	0.57	64.2	33.9	0.47	0.10	HfO <sub>2</sub> :1.25
c	0.32	65.4	32.5	0.20	0.10	-
d	94.6	0.94	1.66	N/A	0.66	-
e	0.37	43.9	36.8	16.7	0.11	HfO <sub>2</sub> :1.43
f	0.08	66.06	N/A	1.58	0.10	N/A

N/A: data not available.

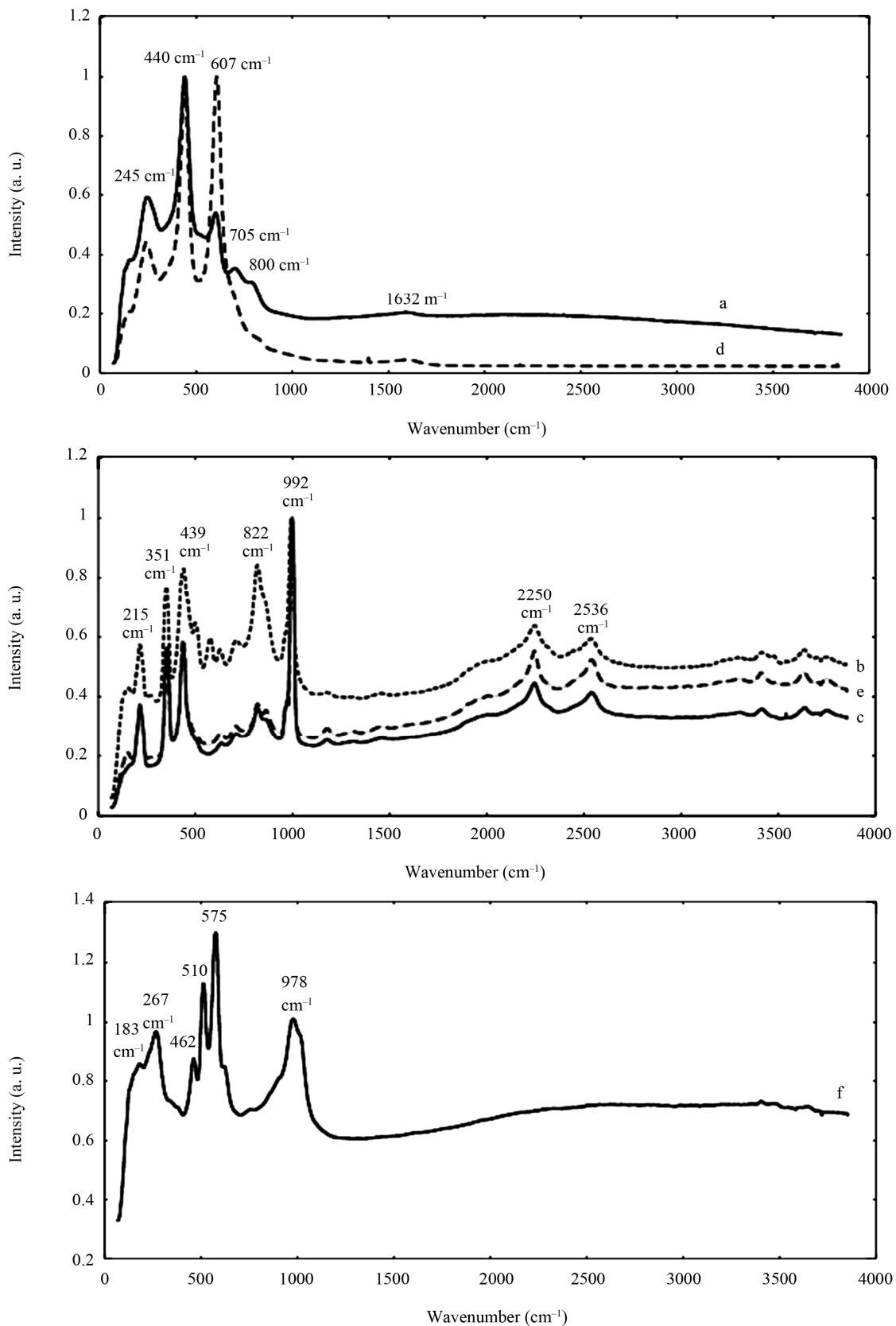


**Figure 2. Raman spectra of the natural rutile (“a” and “d”—top) and zircon powders (“b”, “c”, and “e”—middle, and “f”—bottom). The spectra were offset for clarity.**

**Figure 3.** The main oxygen 1s peaks correspond both to oxidized metal compounds and to a small extent also to oxidized carbon components in the layer of atmospheric surface contamination. The oxygen peaks for Fe<sub>2</sub>O<sub>3</sub>/Fe<sub>3</sub>O<sub>4</sub>/

FeO (≈530.2 eV) and TiO<sub>2</sub> (530.0 eV) occurred at similar binding energies and were therefore difficult to distinguish. Therefore, data presented in **Figure 3** is based on the metal content only.

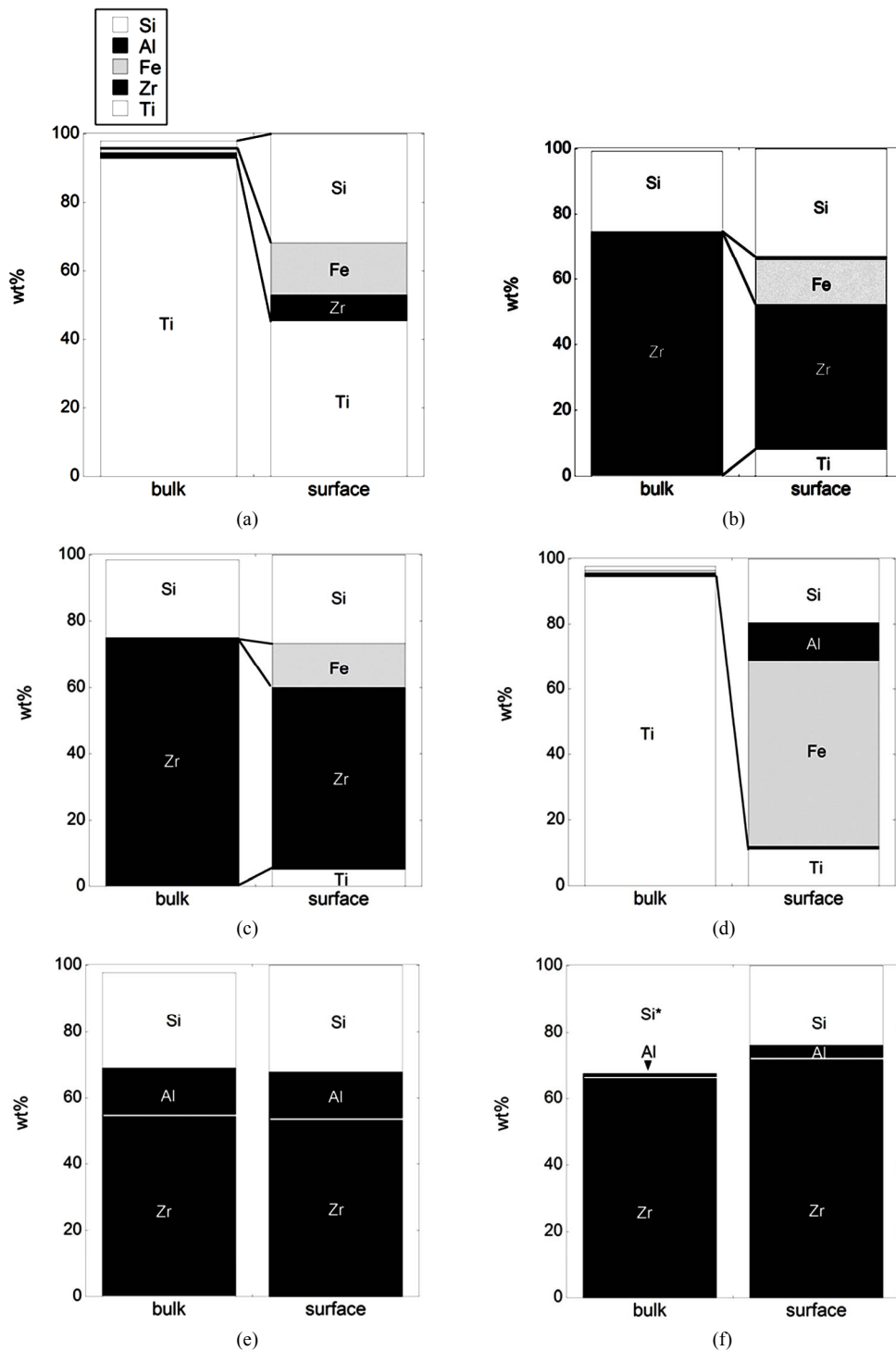


**Figure 3.** Bulk and surface composition based on metals only (no oxides) for the natural rutile ((a) and (d)) and the zircon powders ((b), (c), (e), and (f)). Bulk composition is based on supplier information (Table 5) and surface composition of the outermost surface (<5 nm) is based on XPS results. “Si\*” shown for the powder (f) indicates that no bulk information on Si was available but it is most probably present.

In the case of the zircon powder “f”, where information on the SiO<sub>2</sub> content was not available, it can be expected that the major part of the remaining composition to 100 wt% is Si, as for the other zircon particles “b”, “c”, and “e”, also indicated by the Raman results and by the surface compositional analysis. As expected, the bulk metal composition consisted mainly of titanium in the case of the rutile powders “a” and “d”, and of zirconium and silicon (ZrSiO<sub>4</sub>) in the case of the zircon powders “b”, “c”, “e”, and “f”. In addition, the zircon powders “e” and “f” also contained a small amount of Al. The surface metal composition (<5 nm) was however significantly different for the powders “a”, “b”, “c”, and “d”, and enriched in oxidized iron, silicon, and aluminium (in the case of particles “d” only) while depleted in oxidized zirconium and titanium, respectively. The zircon powders “e” and “f” revealed similar bulk and surface composition. Contradictory to the findings for the powders “d”, “e”, and “f”, no significant amounts of oxidized aluminium were observed in the surface oxide of the powders of “a”, “b”, and “c”. These findings are, as will be discussed in the following sections, of large importance for the metal release behaviour.

### 3.2. Zirconium and Titanium Release— Dependency on Solution pH, Material, and Solution Chemicals

Consistent with literature findings [3,4,18], the measured release of zirconium and titanium into the five different artificial body fluids of varying pH and complexity, was generally very low after 2 and 24 hours of exposure. Most concentrations measured were close to the limit of detection for titanium (0.12 µg/L) and zirconium (0.34 µg/L), respectively. All materials investigated released less than 4.1 µg/L Ti (powder “f”) and 180.7 µg/L Zr (powder “f”), at rates corresponding to less than 0.00024 µg/cm<sup>2</sup>/h Ti (powder “d”) and 0.0049 µg/cm<sup>2</sup>/h Zr (powder “f”). With the exception of the fine-sized powder “f”, the concentrations and release rates were significantly lower: less than 2.1 µg/L Ti (powder “a”) and 1.6 µg/L Zr (powder “a”), and less than 0.00024 µg/cm<sup>2</sup>/h Ti (powder “d”) and 0.00027 µg/cm<sup>2</sup>/h Zr (powder “b”). It should be noticed that there is a large difference in specific surface area (**Table 1**) and particle diameters (**Table 2**) between the different powders, with the zircon powder “f” having the smallest mean particle size and the largest specific surface area. Nevertheless, the largest amounts of zirconium and silicon were released from this powder, even when normalized to the specific surface area.

The measured release expressed as the released amount of metal per amount of metal loaded, **Figure 4**, allows the possibility to refer to the dissolved percentage of the respective metal (titanium and zirconium). While the measured concentrations of titanium and zirconium were fairly

similar for all materials except powder “f” with slightly higher concentrations of titanium and significantly higher concentrations of zirconium, the released amount normalized to the bulk content of the respective metal gives another picture (**Figure 4**). Most titanium per titanium content, as much as 10% for the “f”-powder and less than 0.3% for the “b”, “c” and “e”-powders, was actually released from the zircon powders (“b”, “c”, “e”, and “f”), and most zirconium per zirconium content was released from the rutile TiO<sub>2</sub> powders (“a” and “d”) with the exception of the zircon powder “f” that also showed the highest amounts of released zirconium (<0.4 wt% of bulk content) between the investigated materials. These results clearly show a selective release/dissolution of impurities. Similar findings have previously been observed for other insoluble powders, where impurities of e.g. iron were released to a larger extent compared with chromium from trivalent insoluble chromium oxide particles into artificial lysosomal fluid (ALF, the same fluid as used in this study) [32]. This could be a result of less stable incorporation of impurities within the matrix. Other findings have shown a higher release of nickel when incorporated in a structure of stainless steel of lower solubility to nickel (ferrite) compared with a structure of higher solubility of nickel (austenite) [33]. Another more obvious reason could be that some impurities were enriched at the surface, as evident from **Figure 3**. The surface enrichment of the impurity elements Ti or Zr was clearly seen for the powders “a”, “b”, and “c”, but not for the other powders (**Figure 3**). Another possible reason for the selective release of impurities can be that there is a critical amount of bulk concentration required to form a stable surface oxide. This phenomenon is well known for alloys such as stainless steel, where a critical bulk concentration of about 11 to 13 wt% of chromium is necessary to form a stable mixed Fe<sub>2</sub>O<sub>3</sub>/Cr<sub>2</sub>O<sub>3</sub> surface oxide [34]. It is difficult to compare alloys with bulk oxide materials, which are in their stable thermodynamic form, but as will be seen in the next section, the amount of aluminium oxide in the bulk may play a decisive role for the entire dissolution/release process.

The very low release of titanium and zirconium (rutile TiO<sub>2</sub> powders “a” and “d”: <0.004% of Ti content; zircon powders “b”, “c”, and “e”: <0.002% of Zr content; micronized zircon powder “f”: <0.36% of Zr content) is in agreement with literature findings (if not indicated differently, exposure temperature and solutions are similar to this study) showing rates lower than 0.0005 µg/cm<sup>2</sup>/h Ti (surface of rutile structure on implants) [5], non-detectable amounts of Ti released from massive rutile TiO<sub>2</sub> [2] and micron-sized Ti particles [1], less than 1.2 wt% dissolved for micron-sized rutile TiO<sub>2</sub> particles (7 M nitric acid, in an autoclave) [3], and non-detectable amounts of zirconium released from micron-sized zircon powders

into water at pH 5 [4]. For comparison, the release of titanium from commercially pure (c.p.) titanium and titanium alloy used for implants into similar solutions has been reported significantly higher, less than 4.6 wt% dissolved [18].

All reported investigations, and also this study, measure the dissolved concentration of metal ions or metal species in fluids after different time periods. However, the released fraction that precipitates as insoluble phases is seldom measured. Precipitation processes in water systems are known for zirconium [4,35] but are expected to be negligible at a solution pH lower than 3 [35]. This means, that it would be of major importance for the measured release of zirconium in this study. Despite the expected high release of zirconium in Gastric fluid (GST) at pH 1.5 when considering the pH dependence of the solubility in the zirconium-water system, all particles, with the exception of the fine-sized zircon powder “f”, revealed non-detectable concentrations in GST. In addition, the measured concentration of zirconium increased with time (Figure 4) in all cases (with the exception of some concentrations close to the limit of detection). This implies that precipitation processes, if any, are slower than the metal release process. However, in the weakly alkaline (pH 7.4) solutions, the measured concentrations of zirconium were always slightly lower (often non-detectable) after 24 hours compared with 2 hours of exposure, although most values are close to the detection limit. These findings imply that vital precipitation processes are taking place at this pH level.

It is evident from observed metal release findings that the solution composition is more important than the solution pH for the release of zirconium for all particles in-

vestigated. With some exceptions, this was in contrast to the other metals released (titanium, silicon, iron, and aluminium), (Figure 5), further discussed in the following section. The fluids of ALF (pH 4.5) and GMB (pH 7.4) seemed to be more aggressive compared with the other solutions. This observation became evident when comparing the release of zirconium into ALF and GST (pH 1.5), with always a larger extent of release in ALF compared to GST, despite the expected higher solubility in the fluid of lower pH. When comparing the two solutions at weakly alkaline conditions (pH 7.4), GMB and PBS, the release of zirconium into PBS was non-detectable with one exception (powder “f” after 2 hours), while its release into GMB was detectable for all powders after at least one exposure period. GMB and ALF are both solutions simulating lung fluids, normal deep lung conditions and inflammatory conditions, respectively. Both solutions are of relatively high complexity when considering the number of chemical components and contain citrate or citric acid, ALF at a very high concentration (20.8 g/L citric acid and 0.077 g/L sodium citrate) and GMB at significantly lower concentration (0.097 g/L sodium citrate). Zirconium-citrate complexes are very stable at pH values below 7 and expected at a pH less than 8 [35]. Higher amounts of released zirconium in GMB and ALF compared to the other fluids investigated could have two probable reasons: i) stabilization of soluble zirconium by citrate in the solution (hence, avoiding precipitation) and ii) citrate-induced dissolution of oxidized zirconium. The latter seems more reasonable, at least in the case of ALF (pH 4.5), since no or limited precipitants are expected in the GST solution of very low pH (1.5), which resulted in lower concentrations of released zirconium compared with ALF for all powders.

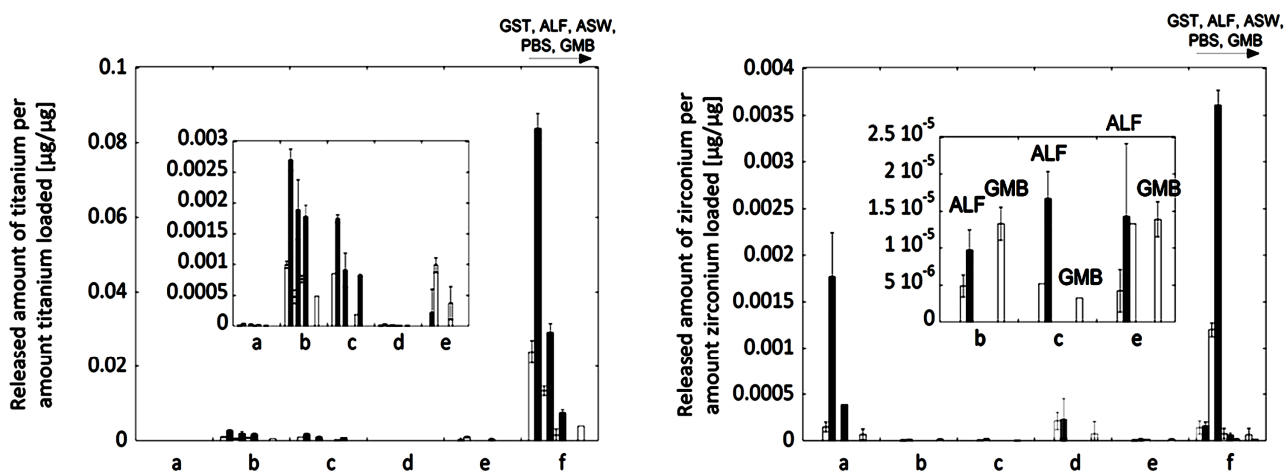


Figure 4. Released amount of metal per amount metal loaded [ $\mu\text{g}/\mu\text{g}$ ] (corresponding to the dissolved percentage of that metal) for titanium (left) and zirconium (right) of the natural rutile (“a” and “d”) and the zircon powders (“b”, “c”, “e”, and “f”). For each material, the release into all fluids with increasing pH (GST, pH 1.5; ALF, pH 4.5; ASW, pH 6.5; PBS, pH 7.4; GMB, pH 7.4) is shown after 2 hours (white bars) and 24 hours (grey bars) of exposure. Specific surface areas are 3.16, 1.19, 1.03, 0.84, 0.65, 5.97  $\text{m}^2/\text{g}$  for the particles “a”, “b”, “c”, “d”, “e”, and “f”, respectively.

### 3.3. Release of Total Metals—Dependency on pH and Surface Structure

While the measured release of titanium and zirconium generally was very low, the release of other metals (silicon, iron and aluminium) was generally significantly higher (Figure 5). The release of all five metals (denoted total metal release) was strongly pH, solution, and material dependent. For powders “a”, “b”, and “c”, the total release of metals decreased with decreasing solution pH, mainly due to the high release of silicon at near-neutral pH conditions. The total metal release into PBS and GMB (both pH 7.4) was in these cases also significantly higher (factor 3 - 24) compared to the total release from the other powders “d”, “e”, and “f”, when normalized to the specific surface areas. The non-proportional release of silicon at near-neutral pH, also observed in previous zircon dissolution studies [4], could be attributed both to the selective release of silicon and to precipitation of zirconium species, as previously discussed. Selective release of silicon would be in concordance with the enrichment of oxidized silicon on the surface for the powders of “a”, “b”, “c”, and “d” (Figure 3) and similar to the selective release of other metals observed for alloy particles and

oxide particles into the same solutions [32,36,37].

In contrast, the pH dependence of the total amount of metals released for powders “d”, “e”, and “f” showed the opposite results, with increasing metal release with decreasing pH. At the same time, the release of silicon was significantly less relevant for the total metal release compared with the “a”, “b”, and “c” powders and the release of iron and aluminium more important in the ALF and GST fluids (pH 4.5 and pH 1.5, respectively). In the case of the “c”, “e”, and “f” (all zircons) powders, the total metal release was higher in ALF compared with ASW (pH 6.5) and GST (pH 1.5), results not expected from the general pH dependence. As previously discussed for zirconium, the complexation ability of ALF (with high amounts of citric acid) could be important. It has previously been shown that the complexation ability of citric acid in ALF is the main factor governing the release of metals from stainless steel particles [19].

To explain the similar metal release behaviour (pH dependence) of the powders “a”, “b”, and “c”, in contrast to the contradictory behaviour of particles “d”, “e”, and “f”, similarities between the powders of each group were identified.

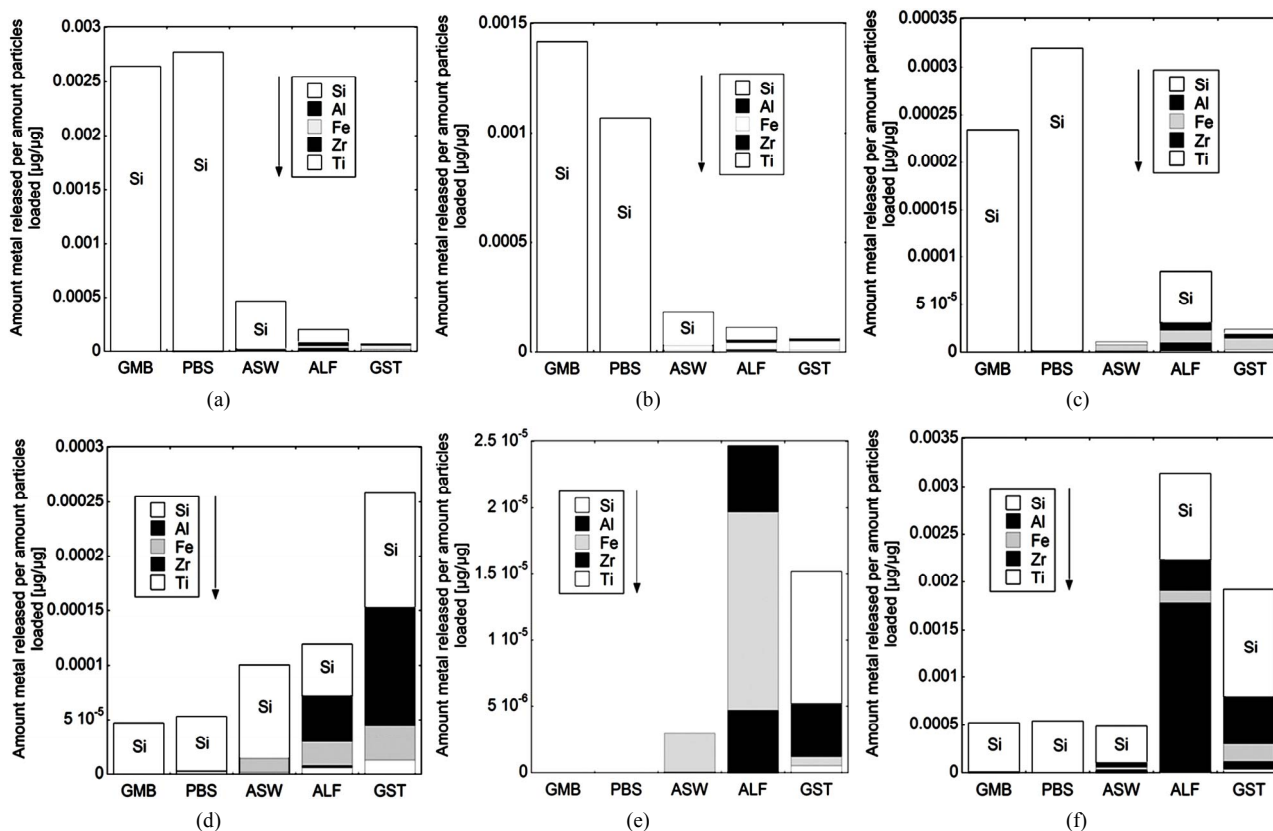


Figure 5. Total amount of released metal (Ti, Zr, Fe, Al, and Si) per amount of powders loaded [µg/µg] after 24 hours of exposure for the natural rutile ((a) and (d)), and zircon powders ((b), (c), (e), and (f)), into the different synthetic body fluids with decreasing pH (GMB, pH 7.4; PBS, pH 7.4; ASW, pH 6.5; ALF, pH 4.5; GST, pH 1.5). Note the difference of the scales. Specific surface areas are 3.16, 1.19, 1.03, 0.84, 0.65, 5.97 m<sup>2</sup>/g for the powders (a), (b), (c), (d), (e), and (f), respectively.

The same material components, rutile TiO<sub>2</sub> and zircon (ZrSiO<sub>4</sub>), confirmed by Raman spectroscopy and bulk composition, c.f. **Figures 2** and **3**, were present in both groups with one natural rutile powder and two zircon powders, respectively. However, there were clear similarities for the “a”, “b”, and “c” powders, and for the “d”, “e”, and “f” powders, respectively, when considering the surface composition (**Figure 3**). No significant amounts of oxidized aluminium was observed in the surface oxide of the “a”, “b”, and “c” powders, whereas present for the “d”, “e”, and “f” powders. Aluminium oxide is most soluble at low pH while oxidized silicon is most soluble at the highest pH investigated (pH 7.4). For alloys it is known that a stable mixed surface oxide (that combines the positive material properties of each oxide) forms when exceeding a critical bulk and hence surface composition. This is for example true for stainless steels where the bulk chromium content has to exceed 11 - 13 wt% in order to form a stable mixed Fe<sub>2</sub>O<sub>3</sub>/Cr<sub>2</sub>O<sub>3</sub> oxide layer which is protective in most ambient environments at both low and high pH (Fe<sub>2</sub>O<sub>3</sub> would dissolve at low pH and Cr<sub>2</sub>O<sub>3</sub> at high pH) [34].

It is therefore proposed that the different metal release behaviour between the “d”, “e”, and “f”-powders compared to the “a”, “b”, and “c” powders is due to the presence of a mixed surface oxide of silicon and aluminium. Its presence would explain why silicon for these materials mostly was released at acidic conditions, opposite to its natural pH dependence. At acidic conditions degradation of this mixed oxide could take place with the increased release of aluminium and silicon as consequence (clearly observed for these particles, **Figure 5** bottom). However, to prove the presence of this mixed surface oxide and this hypothesis, other very surface-sensitive techniques are required that are able to analyse the structure and phase of the outermost (<5 nm or less) surface.

Since phagocytosed (<5 µm) particles (for instance pigments of rutile TiO<sub>2</sub> and ZrO<sub>2</sub>) previously have shown to be toxic in several studies [1,8], increasingly with increasing volume of particles (below that size limit) [8], the release of metals from particles engulfed by cells (high complexing capacity and lower pH) may be an important mechanism, as previously suggested for nanoparticles of different materials by a Trojan-horse type mechanism [38,39]. The particles studied in this study are larger than 5 µm (median size about 100 to 130 µm) with the exception of powder “f” (median size of 2 µm), but the release behaviour studied may be of importance for smaller particles as well. It was also shown in the case of the zircon powders that the size is important for the metal release. An in-depth understanding of the complexity of the metal release behaviour of the different rutile and zircon powders is therefore shown to be governed by 1) surface composition, phases, and structure, 2) size, 3) presence

of impurities, 4) solution pH, and 5) solution complexation ability.

#### 4. Conclusions

The release of zirconium, titanium, aluminum, iron, and silicon from different micron-sized natural rutile (TiO<sub>2</sub>, 2 types) and zircon (ZrSiO<sub>4</sub>, 4 types) powders was investigated. The importance of bulk and surface composition for the release mechanisms into five different synthetic body fluids was emphasized, covering a pH range from 1.5 to 7.4 (hence different possible endpoints), and different solution complexities (artificial gastric fluid (GST, pH 1.5), artificial lysosomal fluid (ALF, pH 4.5), artificial sweat (ASW, pH 6.5), phosphate buffered saline (PBS, pH 7.4), and Gamble’s solution (GMB, pH 7.4)). The following main conclusions were drawn:

- The surface oxide composition revealed the enrichments of minor bulk elements for both natural rutile (TiO<sub>2</sub>) powders and two zircon powders, but not for the other two zircon powders. One of the rutile and two of the zircon powders showed a significant amount of oxidized aluminum in the surface oxide which probably determines their different release behavior.
- Generally, very low amounts of released titanium and zirconium from both natural rutile and zircon powders. Their release is selective when present as a minor element. While the release of titanium is strongly pH dependent (increasing with decreasing pH), the measured release of zirconium is caused by complexation processes (increasing in complexing solutions) and precipitation processes (at near-neutral pH).
- The total metal release was dominated by silicon in near-neutral solutions. The release of titanium, iron, aluminum, and zirconium increased with decreasing pH, but was also dependent on the complexation ability of the solution (especially for zirconium).
- The total metal release decreased with decreasing pH for the powders with no significant amounts of oxidized aluminum in the surface oxide. In contrast, the total metal release is increasing with decreasing pH for the powders with a stable mixed surface oxide rich in silicon and aluminum.
- To conclude, the metal release behavior for natural rutile and zircon powders is determined by 1) surface composition, phases, and structure; 2) size; 3) impurities; 4) solution pH; and 5) solution complexation ability.

#### 5. Acknowledgements

Rio Tinto Iron & Titanium and Exxaro Resources Ltd are acknowledged for commissioning the study of Bioaccessibility of zirconium and titanium released from different zircon and rutile products in synthetic biological media.

Cusanuswerk, Germany, is acknowledged for the financing of Yolanda Hedberg. Dr. Eric Tyrode is acknowledged for providing his Raman instrument. Instrumental grants from Knut and Alice Wallenberg foundation for the XPS instrument are acknowledged.

## REFERENCES

- [1] R. Kumazawa, F. Watari, N. Takashi, Y. Tanimura, M. Uo and Y. Totsuka, "Effects of Ti Ions and Particles on Neutrophil Function and Morphology," *Biomaterials*, Vol. 23, No. 17, 2002, pp. 3757-3764. [doi:10.1016/S0142-9612\(02\)00115-1](https://doi.org/10.1016/S0142-9612(02)00115-1)
- [2] J. Li, "Behaviour of Titanium and Titania-Based Ceramics *in Vitro* and *in Vivo*," *Biomaterials*, Vol. 14, No. 3, 1993, pp. 229-232. [doi:10.1016/0142-9612\(93\)90028-Z](https://doi.org/10.1016/0142-9612(93)90028-Z)
- [3] S. Snäll and T. Liljefors, "Leachability of Major Elements from Minerals in Strong Acids," *Journal of Geochemical Exploration*, Vol. 71, No. 1, 2000, pp. 1-12. [doi:10.1016/S0375-6742\(00\)00139-4](https://doi.org/10.1016/S0375-6742(00)00139-4)
- [4] M. P. Tole, "The Kinetics of Dissolution of Zircon (ZrSiO<sub>4</sub>)," *Geochimica et Cosmochimica Acta*, Vol. 49, No. 2, 1985, pp. 453-458. [doi:10.1016/0016-7037\(85\)90036-5](https://doi.org/10.1016/0016-7037(85)90036-5)
- [5] A. Wisbey, P. J. Gregson, L. M. Peter and M. Tuke, "Effect of Surface Treatment on the Dissolution of Titanium-Based Implant Materials," *Biomaterials*, Vol. 12, No. 5, 1991, pp. 470-473. [doi:10.1016/0142-9612\(91\)90144-Y](https://doi.org/10.1016/0142-9612(91)90144-Y)
- [6] G. Vallés, P. González-Melendi, J. L. González-Carrasco, L. Saldaña, E. Sánchez-Sabaté, L. Munuera and N. Vilaboa, "Differential Inflammatory Macrophage Response to Rutile and Titanium Particles," *Biomaterials*, Vol. 27, No. 30, 2006, pp. 5199-5211. [doi:10.1016/j.biomaterials.2006.05.045](https://doi.org/10.1016/j.biomaterials.2006.05.045)
- [7] T. J. Brunner, P. Wick, P. Manser, P. Spohn, R. N. Grass, L. K. Limbach, A. Bruinink and W. J. Stark, "In Vitro Cytotoxicity of Oxide Nanoparticles: Comparison to Asbestos, Silica, and the Effect of Particle Solubility," *Environmental Science & Technology*, Vol. 40, No. 14, 2006, pp. 4374-4381. [doi:10.1021/es052069j](https://doi.org/10.1021/es052069j)
- [8] A. Yamamoto, R. Honma, M. Sumita and T. Hanawa, "Cytotoxicity Evaluation of Ceramic Particles of Different Sizes and Shapes," *Journal of Biomedical Materials Research Part A*, Vol. 68A, No. 2, 2004, pp. 244-256. [doi:10.1002/jbm.a.20020](https://doi.org/10.1002/jbm.a.20020)
- [9] Y. Duan, J. Liu, L. Ma, N. Li, H. Liu, J. Wang, L. Zheng, C. Liu, X. Wang, X. Zhao, J. Yan, S. Wang, H. Wang, X. Zhang and F. Hong, "Toxicological Characteristics of Nanoparticulate Anatase Titanium Dioxide in Mice," *Biomaterials*, Vol. 31, No. 5, 2010, pp. 894-899. [doi:10.1016/j.biomaterials.2009.10.003](https://doi.org/10.1016/j.biomaterials.2009.10.003)
- [10] R. Hu, X. Gong, Y. Duan, N. Li, Y. Che, Y. Cui, M. Zhou, C. Liu, H. Wang and F. Hong, "Neurotoxicological Effects and the Impairment of Spatial Recognition Memory in Mice Caused by Exposure to TiO<sub>2</sub> Nanoparticles," *Biomaterials*, Vol. 31, No. 31, 2010, pp. 8043-8050. [doi:10.1016/j.biomaterials.2010.07.011](https://doi.org/10.1016/j.biomaterials.2010.07.011)
- [11] L. Ma, J. Liu, N. Li, J. Wang, Y. Duan, J. Yan, H. Liu, H. Wang and F. Hong, "Oxidative Stress in the Brain of Mice Caused by Translocated Nanoparticulate TiO<sub>2</sub> Delivered to the Abdominal Cavity," *Biomaterials*, Vol. 31, No. 1, 2010, pp. 99-105. [doi:10.1016/j.biomaterials.2009.09.028](https://doi.org/10.1016/j.biomaterials.2009.09.028)
- [12] H. L. Karlsson, J. Gustafsson, P. Cronholm and L. Möller, "Size-Dependent Toxicity of Metal Oxide Particles—A Comparison between Nano- and Micrometer Size," *Toxicology Letters*, Vol. 188, No. 2, 2009, pp. 112-118. [doi:10.1016/j.toxlet.2009.03.014](https://doi.org/10.1016/j.toxlet.2009.03.014)
- [13] D. B. Warheit, T. R. Webb, C. M. Sayes, V. L. Colvin and K. L. Reed, "Pulmonary Instillation Studies with Nanoscale TiO<sub>2</sub> Rods and Dots in Rats: Toxicity Is Not Dependent upon Particle Size and Surface Area," *Toxicological Sciences*, Vol. 91, No. 1, 2006, pp. 227-236. [doi:10.1093/toxsci/kfj140](https://doi.org/10.1093/toxsci/kfj140)
- [14] C. M. Sayes, R. Wahi, P. A. Kurian, Y. Liu, J. L. West, K. D. Ausman, D. B. Warheit and V. L. Colvin, "Correlating Nanoscale Titania Structure with Toxicity: A Cytotoxicity and Inflammatory Response Study with Human Dermal Fibroblasts and Human Lung Epithelial Cells," *Toxicological Sciences*, Vol. 92, No. 1, 2006, pp. 174-185. [doi:10.1093/toxsci/kfj197](https://doi.org/10.1093/toxsci/kfj197)
- [15] J.-R. Gurr, A. S. S. Wang, C.-H. Chen and K.-Y. Jan, "Ultrafine Titanium Dioxide Particles in the Absence of Photoactivation Can Induce Oxidative Damage to Human Bronchial Epithelial Cells," *Toxicology*, Vol. 213, No. 1-2, 2005, pp. 66-73. [doi:10.1016/j.tox.2005.05.007](https://doi.org/10.1016/j.tox.2005.05.007)
- [16] J.-X. Wang, Y.-B. Fan, Y. Gao, Q.-H. Hu and T.-C. Wang, "TiO<sub>2</sub> Nanoparticles Translocation and Potential Toxicological Effect in Rats after Intraarticular Injection," *Biomaterials*, Vol. 30, No. 27, 2009, pp. 4590-4600. [doi:10.1016/j.biomaterials.2009.05.008](https://doi.org/10.1016/j.biomaterials.2009.05.008)
- [17] S. M. Hussain, K. L. Hess, J. M. Gearhart, K. T. Geiss and J. J. Schlager, "In Vitro Toxicity of Nanoparticles in BRL 3A Rat Liver Cells," *Toxicology in Vitro*, Vol. 19, No. 7, 2005, pp. 975-983. [doi:10.1016/j.tiv.2005.06.034](https://doi.org/10.1016/j.tiv.2005.06.034)
- [18] T. Mumme, R. Müller-Rath, N. Jakobi, M. Weißkopf, W. Dott, R. Marx and D.-C. Wirtz, "In Vitro Serum Levels of Metal Ions Released from Orthopaedic Implants," *European Journal of Orthopaedic Surgery and Traumatology*, Vol. 15, No. 2, 2011, pp. 1099-1114. [doi:10.1007/s00590-004-0206-6](https://doi.org/10.1007/s00590-004-0206-6)
- [19] Y. Hedberg, J. Hedberg, Y. Liu and I. Odnevall Wallinder, "Complexation- and Ligand-Induced Metal Release from 316L Particles: Dependence on Particle Size and Crystallographic Structure," *BioMetals*, Vol. 24, No. 6, 2005, pp. 83-89. [doi:10.1007/s10534-011-9469-7](https://doi.org/10.1007/s10534-011-9469-7)
- [20] D. T. H. Wassell and G. Embery, "Adsorption of Bovine Serum Albumin on to Titanium Powder," *Biomaterials*, Vol. 17, No. 9, 1996, pp. 859-864. [doi:10.1016/0142-9612\(96\)83280-7](https://doi.org/10.1016/0142-9612(96)83280-7)
- [21] B. Wälivaara, B.-O. Aronsson, M. Rodahl, J. Lausmaa and P. Tengvall, "Titanium with Different Oxides: In Vitro Studies of Protein Adsorption and Contact Activation," *Biomaterials*, Vol. 15, No. 10, 1994, pp. 827-834. [doi:10.1016/0142-9612\(94\)90038-8](https://doi.org/10.1016/0142-9612(94)90038-8)
- [22] E. Tyrode, M. W. Rutland and C. D. Bain, "Adsorption of CTAB on Hydrophilic Silica Studied by Linear and Non-linear Optical Spectroscopy," *Journal of the American Chemical Society*, Vol. 117, No. 1, 1995, pp. 100-105. [doi:10.1021/ja00077a011](https://doi.org/10.1021/ja00077a011)

- mical Society*, Vol. 130, No. 51, 2008, pp. 17434-17445.  
[doi:10.1021/ja805169z](https://doi.org/10.1021/ja805169z)
- [23] W. Stopford, J. Turner, D. Cappellini and T. Brocka, "Bioaccessibility Testing of Cobalt Compounds," *Journal of Environmental Monitoring*, Vol. 5, No. 4, 2003, pp. 675-680. [doi:10.1039/b302257a](https://doi.org/10.1039/b302257a)
- [24] EN 1811, "Test Method for Release of Nickel from Products Intended to Come into Direct and Prolonged Contact with the Skin," 1998.
- [25] A. de Meringo, C. Morscheidt, S. Thélohan and H. Tiesler, "In Vitro Assessment of Biodurability: Acellular Systems," *Environmental Health Perspectives*, Vol. 102, No. 5, 1994, pp. 1-6.
- [26] S. C. Hamel, B. Buckley and P. J. Lioy, "Bioaccessibility of Metals in Soils for Different Liquid to Solid Ratios in Synthetic Gastric Fluid," *Environmental Science & Technology*, Vol. 32, No. 3, 1998, pp. 358-362.  
[doi:10.1021/es9701422](https://doi.org/10.1021/es9701422)
- [27] M. Ocaña, V. Fornés, J. V. G. Ramos and C. J. Serna, "Factors Affecting the Infrared and Raman Spectra of Rutile Powders," *Journal of Solid State Chemistry*, Vol. 75, No. 2, 1988, pp. 364-372. [doi:10.1016/0022-4596\(88\)90176-4](https://doi.org/10.1016/0022-4596(88)90176-4)
- [28] S.-M. Oh and T. Ishigaki, "Preparation of Pure Rutile and Anatase TiO<sub>2</sub> Nanopowders Using RF Thermal Plasma," *Thin Solid Films*, Vol. 457, No. 1, 2004, pp. 186-191.  
[doi:10.1016/j.tsf.2003.12.043](https://doi.org/10.1016/j.tsf.2003.12.043)
- [29] V. Swamy, B. C. Muddle and Q. Dai, "Size-Dependent Modifications of the Raman Spectrum of Rutile TiO<sub>2</sub>," *Applied Physics Letters*, Vol. 89, No. 16, 2006, pp. 163118-163120. [doi:10.1063/1.2364123](https://doi.org/10.1063/1.2364123)
- [30] R. W. G. Syme, D. Lockwood and H. Kerr, "Raman Spectrum of Synthetic Zircon (ZrSiO<sub>4</sub>) and Thorite (ThSiO<sub>4</sub>)," *Journal of Physics C: Solid State Physics*, Vol. 10, No. 8, 1977, pp. 1335-1348. [doi:10.1088/0022-3719/10/8/036](https://doi.org/10.1088/0022-3719/10/8/036)
- [31] G. G. Siu, M. J. Stokes and Y. Liu, "Variation of Fundamental and Higher-Order Raman Spectra of ZrO<sub>2</sub> Nanograins with Annealing Temperature," *Physical Review B*, Vol. 59, No. 4, 1999, pp. 3173-3179.  
[doi:10.1103/PhysRevB.59.3173](https://doi.org/10.1103/PhysRevB.59.3173)
- [32] Y. Hedberg, J. Gustafsson, H. L. Karlsson, L. Möller and I. Odnevall Wallinder, "Bioaccessibility, Bioavailability and Toxicity of Commercially Relevant Iron- and Chromium-Based Particles: In Vitro Studies with an Inhalation Perspective," *Particle and Fibre Toxicology*, Vol. 7, 2010, p. 23. [doi:10.1186/1743-8977-7-23](https://doi.org/10.1186/1743-8977-7-23)
- [33] Y. Hedberg, O. Karlsson, P. Szakalos and I. Odnevall Wallinder, "Ultrafine 316 L Stainless Steel Particles with Frozen-In Magnetic Structures Characterized by Means of Electron Backscattered Diffraction," *Materials Letters*, Vol. 65, No. 14, 2011, pp. 2089-2092.  
[doi:10.1016/j.matlet.2011.04.019](https://doi.org/10.1016/j.matlet.2011.04.019)
- [34] A. J. Sedriks, "Corrosion of Stainless Steels," 2nd Edition, John Wiley & Sons, Inc., New York, 1996.
- [35] J.-H. Choy and Y.-S. Han, "Citrate Route to the Piezoelectric Pb(Zr,Ti)O<sub>3</sub> Oxide," *Journal of Materials Chemistry*, Vol. 7, No. 9, 1997, pp. 1815-1820.  
[doi:10.1039/a700687j](https://doi.org/10.1039/a700687j)
- [36] Y. Hedberg, K. Midander and I. Odnevall Wallinder, "Particles, Sweat, and Tears: A Comparative Study on Bioaccessibility of Ferrocromium Alloy and Stainless Steel Particles, the Pure Metals and Their Metal Oxides, in Simulated Skin and Eye Contact," *Integrated Environmental Assessment and Management*, Vol. 6, No. 3, 2010, pp. 456-468. [doi:10.1002/ieam.66](https://doi.org/10.1002/ieam.66)
- [37] K. Midander, A. de Frutos, Y. Hedberg, G. Darrie and I. Odnevall Wallinder, "Bioaccessibility Studies of Ferrocromium Alloy Particles for a Simulated Inhalation Scenario: A Comparative Study with the Pure Metals and Stainless Steel," *Integrated Environmental Assessment and Management*, Vol. 6, No. 3, 2010, pp. 441-455.  
[doi:10.1002/ieam.32](https://doi.org/10.1002/ieam.32)
- [38] H. L. Karlsson, P. Cronholm, J. Gustafsson and L. Möller, "Copper Oxide Nanoparticles Are Highly Toxic: A Comparison between Metal Oxide Nanoparticles and Carbon Nanotubes," *Chemical Research in Toxicology*, Vol. 21, No. 9, 2008, pp. 1726-1732. [doi:10.1021/tx800064j](https://doi.org/10.1021/tx800064j)
- [39] L. K. Limbach, P. Wick, P. Manser, R. N. Grass, A. Brunink and W. J. Stark, "Exposure of Engineered Nanoparticles to Human Lung Epithelial Cells: Influence of Chemical Composition and Catalytic Activity on Oxidative Stress," *Environmental Science & Technology*, Vol. 41, No. 11, 2007, pp. 4158-4163. [doi:10.1021/es062629t](https://doi.org/10.1021/es062629t)